PCCP

Cite this: *Phys. Chem. Chem. Phys.*, 2012, **14**, 5919–5923

www.rsc.org/pccp

COMMUNICATION

Application of surface enhanced Raman spectroscopy to the study of SOFC electrode surfaces†

Xiaxi Li,[a] Kevin Blinn,[a] Yingcui Fang,‡[a] Mingfei Liu,[a] Mahmoud A. Mahmoud,[b] Shuang Cheng,§[a] Lawrence A. Bottomley,[b] Mostafa El-Sayed[b] and Meilin Liu*[a]

Received 10th January 2012, Accepted 6th February 2012
DOI: 10.1039/c2cp40091j

SERS provided by sputtered silver was employed to detect trace amounts of chemical species on SOFC electrodes. Considerable enhancement of Raman signal and lowered detection threshold were shown for coked nickel surfaces, CeO_2 coatings, and cathode materials (LSM and LSCF), suggesting a viable approach to probing electrode degradation and surface catalytic mechanism.

While solid oxide fuel cells (SOFCs) offer a promising solution for efficient, direct conversion of a wide variety of chemical fuels to electricity,[1,2] they are yet to be commercialized on a large scale. The obstacles to commercialization include high cost associated with the high operation temperature required to enhance electrode activity and inadequate stability due to materials degradation. To make SOFC technologies economically competitive, a fundamental understanding of the reaction mechanism(s) taking place at the SOFC electrode surface is required to rationally design more efficient materials at low cost. By understanding how the electrochemical reactions are catalyzed and how the electrode loses activity over time, researchers may be able to tailor the materials for best performance and stability of SOFCs.

To address the issue of insufficient electrode activity, surface modifications have been widely employed in SOFC electrodes. For example, decorating an $La_{1-x}Sr_xCo_{1-y}Fe_yO_{3-\delta}$ (LSCF) cathode backbone with certain nanoparticles such as $Sm_{1-x}Sr_xCoO_{3-\delta}$ (SSC) and $Ce_{1-x}Sm_xO_{2-\delta}$ (SDC) reduces the polarization resistance;[3,4] while coating the LSCF surface with $La_{1-x}Sr_xMnO_{3-\delta}$ (LSM) improves the long-term stability.[5] On the other hand, the degradation of the electrodes is usually accompanied by formation of undesired species on the electrode surface, which is particularly prevalent in SOFC anodes, such as the carbon deposition after operating with hydrocarbon fuels[6] as well as nickel sulfide and adsorbed sulfur after being exposed to a sulfur contaminated fuel.[7–9]

Both effective modification agents and degradation-induced species could be present in trace amounts, which become extremely hard to detect using conventional characterization tools due either to lack of chemical sensitivity and surface specificity or to limited applicability under *in-situ* conditions. Vibrational spectroscopy, a family of techniques including Raman and FTIR, is sensitive to chemical structure and has been successfully employed to study SOFC electrodes previously.[8,10–15] In particular, under the right conditions, Raman spectroscopy is able to inspect the phase evolution and reaction intermediates on the very top of the electrode surface.[16,17] However, the inherently low sensitivity of Raman precludes probing species present in trace amounts on the SOFC surface that are connected to cell performance.

Surface enhanced Raman spectroscopy (SERS) has been recognized as a powerful tool in analytical chemistry, particularly for identification of chemicals adsorbed onto the surface of coinage metals like Au, Ag, and Cu.[18,19] However, we are unaware of any other application of SERS for the analysis of SOFC electrodes besides some preliminary exploration in our group.[10] This is likely in part due to the fact that the common electrode materials used in SOFC (*e.g.* Ni and LSM) are not SERS active themselves. Therefore, enhancement must be provided by deposition of coinage metal particles.[20,21] The methodology of applying SERS active materials to enhance the Raman signal of the substrate has been successfully implemented to study graphene and carbon nanotubes,[22–24] the studies of which have similar obstacles to SOFC electrode investigations.

Preliminary results shown by our group have demonstrated SERS on SOFC electrodes through co-deposition of silver with the material of interest by combustion chemical vapor deposition, loading coinage metal colloids and sputtering deposition of silver,[10] following previous techniques developed to introduce SERS for non-coinage metal substrates.[25–27] The co-deposition method cannot be used to study a real SOFC electrode, because the silver is introduced in the fabrication stage and may disturb the electrochemical reaction on the electrode surface. Introducing SERS by metal particle colloids, on the other hand, requires pretreatment of the substrate which may wash out the small amount of species we are interested in, and the stabilizing agents in the colloids may generate misleading Raman peaks. To study the electrode surface with minimal

[a] *School of Materials Science and Engineering, Center for Innovative Fuel Cell and Battery Technologies, Georgia Institute of Technology, Atlanta, GA 30332-0245, USA. E-mail: meilin.liu@mse.gatech.edu*
[b] *School of Chemistry and Biochemistry, Georgia Institute of Technology, Atlanta, Georgia 30332-0400, USA*

† Electronic supplementary information (ESI) available. See DOI: 10.1039/c2cp40091j

‡ Current address: Vacuum Section of Hefei University of Technology, Hefei, Anhui, 230009, People's Republic of China.

§ Current address: School of Physical Science and Technology, Lanzhou University, Lanzhou 730000, People's Republic of China.

disturbances introduced into the system, the physical vapor deposition seems to be the optimal choice.

In this study, DC magnetron sputtering was employed to load silver nanoparticles as the SERS agent, and the parameters were explored to reach an optimal condition for the Raman signal of the underlying substrate. We systematically explored the parameters of the silver sputtering, particularly the working pressure and deposition duration, to reach an optimized condition for SERS. The Raman enhancement was evaluated using standard carbon films fabricated by thermal evaporation. The carbon films exhibited a broad Raman band across 1200 cm^{-1} and 1600 cm^{-1} of relatively uniform intensity; this wide band consists of a D band and a G band that were each significantly broadened due to the amorphous nature of the evaporated carbon films.[28] The enhancement factor (EF) for each sputtering condition was calculated by the ratio of the enhanced peak intensity to the normal intensity of the combined D band and G band. Furthermore, the morphology of the silver overlayers was inspected by SEM and the optical properties by UV-Vis absorption spectroscopy, which were found closely related to the SERS performance. A more detailed discourse of the parameter optimization and the interpretation of the relationship between their physical properties are presented in the ESI.†

The enhancement factors with respect to different loading amounts of silver and the characteristic Raman spectra of the carbon films before and after enhancement are shown in Fig. 1. The EF reached a maximum when the silver loading was appropriate. The EF peaked at a different loading amount depending on the excitation wavelength. The best EF for the 514 nm laser was ~14 with 180 s duration, while the best EF for the 633 nm laser was ~9 with 240 s of silver deposition. The enhanced Raman spectra of carbon for each of these two "optimal" conditions are illustrated in Fig. 1(A) and (B) along with the normal Raman spectra for comparison. These results indicate that the sputtered silver is capable of enhancing the Raman signal of the underlying substrate, and that the enhancement factor can be well controlled by adjusting the sputter parameters. The latter point is discussed in the ESI.†

To compare the silver patterns created in this study with the SERS substrates in other studies, Rhodamine-6G (R6G), a commonly used SERS indicator, was employed. To make sure that the surface concentration of the R6G molecules was well-controlled, equal amounts of R6G solution were loaded into a space on the substrates with a well-defined area. A similar method was used in a previous SERS study, and good uniformity of surface concentration could be attained.[29] The Raman spectra were collected after the evaporation of all the liquids, and a nominal surface concentration could be calculated by dividing the total loading amount by the loading area. As shown in Fig. 2, the characteristic Raman peaks of 7×10^{-12} mol cm^{-2} R6G loaded on the SERS substrate can be distinctively observed; while for the blank substrate, despite the nominal surface concentration being three orders of magnitude higher (7×10^{-9} mol cm^{-2}), the R6G peaks are barely distinguishable. Based on the intensity of main R6G peaks (1390 cm^{-1}), taking into account the surface concentration of R6G molecules, the enhancement factor is estimated to be 4×10^5, which roughly matches figures reported by similar studies.[30] We noticed that the

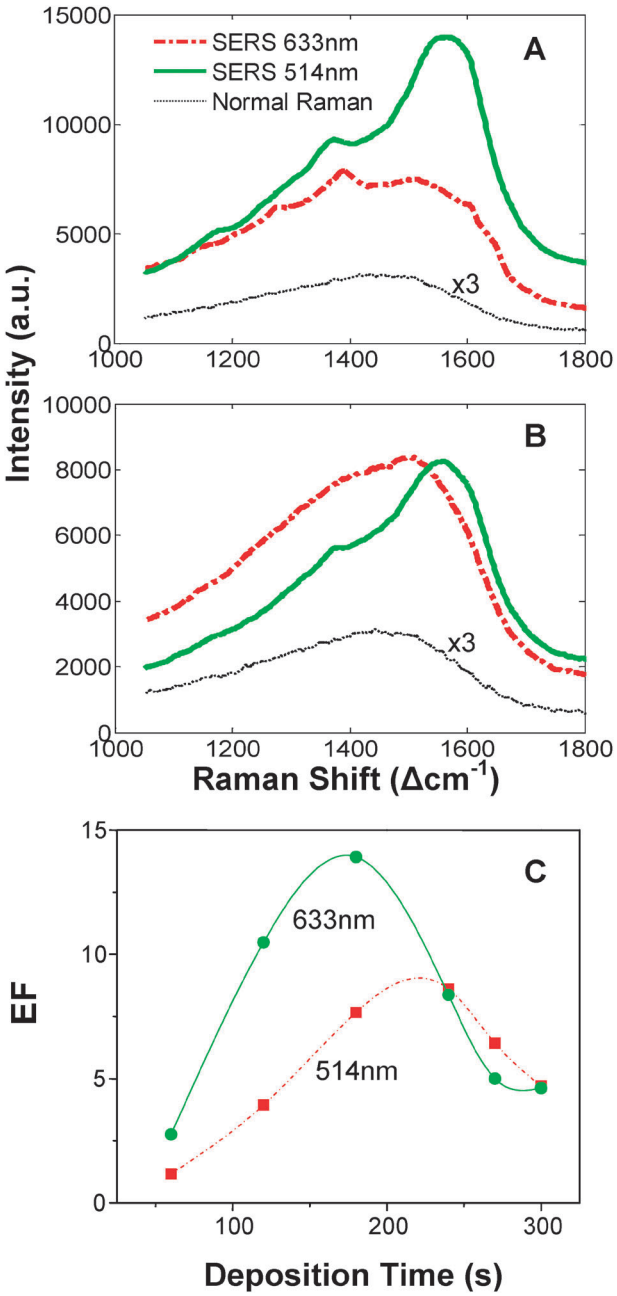

Fig. 1 (A, B) The comparison of SERS spectra and normal Raman spectra of the evaporated carbon film, with 514 nm and 633 nm laser excitations. The SERS is provided by silver depositions of (A) 180 s and (B) 240 s; the normal Raman spectra are magnified by 3 times to display the detailed features of the baselines. (C) The enhancement factors measured from samples with a series of silver deposition times (60 s, 120 s, 180 s, 240 s, 270 s and 300 s); the thin lines in (C) are to guide the eyes.

EF for R6G is several orders of magnitude higher than the EF for carbon. This can be explained by the bulk of the carbon films contributing a large part of the original Raman signal and by the fact that carbon does not selectively adsorb onto the Ag. More discussion on the calculation of enhancement factors is presented in Section B of the ESI.†

The Ag nanoparticle deposition conditions that we found to afford the optimal SERS spectra were 180 s and 240 s deposition

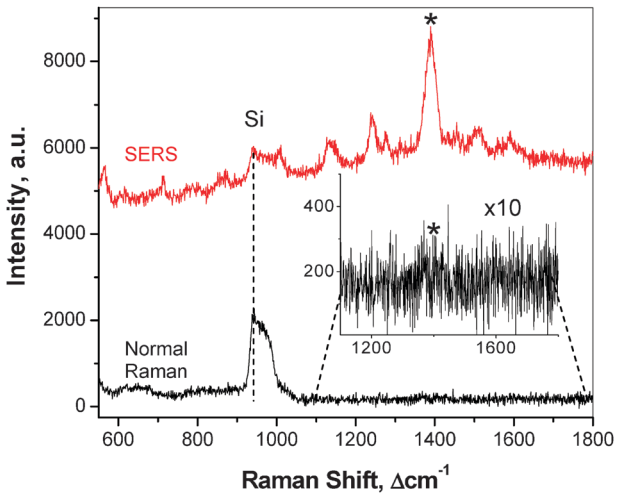

Fig. 2 The Raman spectrum collected from R6G loaded onto SERS substrate (240 s silver loading) with a nominal surface concentration of 7×10^{-12} mol cm^{-2} along with the control spectrum obtained from R6G loaded onto blank silicon with nominal surface concentration of 7×10^{-9} mol cm^{-2}. Inset is a magnification of the control spectrum, showing a weak R6G main peak at 1390 cm^{-1}, which is labeled by (*). The broad hump between 900 cm^{-1} and 1000 cm^{-1} is associated with the silicon substrate.

duration under a working pressure of 2.5 Pa and a target output power of 8 W, for the 514 nm and 633 nm laser excitations, respectively. These conditions were used to apply SERS tests to realistic SOFC material systems. To demonstrate this type of applicability, we chose a coked nickel sample to represent the anode post-operation, the electrochemically deposited CeO_2 on nickel foil as an example of surface modification, and two of the most common cathode materials (LSM and LSCF).

A polished nickel coupon, which was exposed to propane as described in the ESI†, was investigated using normal Raman and SERS with 633 nm excitation. As shown in Fig. 3(A) and (D), patches of carbon deposition formed on the nickel surface. Raman spectra of each of these domains are shown in Fig. 3(B) and (C). Under normal Raman, only the dark region has the carbon signal, while the bright region does not have any features with an appreciable signal-to-noise ratio. After silver deposition for 180 s, the carbon signal in the dark region (Fig. 3C and F) increased by several folds. More prominently, carbon peaks appeared sporadically in the light regions (Fig. 3B and E). The SEM images under high magnification, which were collected before any silver deposition, show that the dark regions were fully covered in carbon, while in the bright region only some white dots formed on the surface, which might be indicative of the early stages of carbon deposition, as shown in Fig. 3(E) and (F). Since these early-stage coking nuclei were only present on part of the light regions, it is consistent with the observation that the carbon peaks on the light region were non-uniformly distributed.

An evaluation of the enhancement factor was performed on the fully developed coke patches. The D band has a net enhancement of 8.8 times and the G band has 8.1 times. This EF value is quite close to what we collected on evaporated carbon ($\sim$7.7 for 633 nm laser excitation). Additionally, the higher enhancement of the D band over the G band is consistent with the theoretical prediction, since the surface plasmon resonance peak wavelength of the silver particles (520 nm) is closer to the D band (691 nm) than the G band (703 nm).

A nominal enhancement factor of the lightly coked regions cannot be reliably estimated because of the lack of background intensity, but it should be much higher than that acquired on the fully coked regions. This enhanced sensitivity to low concentration of carbon implies that once it is optimized, SERS could be a viable approach to detecting incipient phase formation of carbon on anode materials. As is well known, one of the most prominent advantages of SOFCs over other types of fuel cells is the potential for direct conversion to electricity of low-cost hydrocarbon fuels or gasified coal and other carbonaceous fuels (*e.g.*, biomass). To realize this potential, however, the anode must resist coking. Detecting incipient carbon formation on anodes under different conditions is vital to gaining insights into the mechanism of carbon deposition and thus to rational design of coking-tolerant anode materials.

Besides carbon, SERS was applied to other SOFC related materials which are critical for the study of surface chemistry of the electrodes. Shown in Fig. 4(A) is an application of SERS on the detection of cerium oxide, which is used as a modification agent for the nickel anode, a well-studied approach to enhance carbon and sulfur tolerance.[31,32] The very thin layer of CeO_2 could not be clearly identified by either SEM or normal Raman spectroscopy. After the application of the SERS agent, CeO_2 peaks manifested. The capability to detect such a small amount of material will allow us to further investigate the catalytic properties of the surface modification of the SOFC electrodes.

The SERS application on cathode materials is displayed in Fig. 4(B) and (C). The Raman spectra collected from both LSCF pellets and LSM thin film were significantly enhanced after SERS conditioning. It is worth noting that the normal Raman signal of both materials was very weak, because LSCF and LSM belong to the $R\bar{3}c$ space group,[33,34] which represents a near-cubic perovskite phase that has little Raman activity. Since the two materials share a similar phase, their Raman bands are in similar positions. The LSCF signal was enhanced by a rough factor of $\sim$11, and the EF of the LSM signal was $\sim$6.

The surface specificity of SERS was demonstrated by the LSM thin film sputtered on the YSZ substrate. As shown in Fig. 4C, the normal Raman spectrum shows both LSM and YSZ peaks, because a signal was detected from underneath the film since the LSM film was only 100 nm thick. YSZ is much more Raman-active than LSM, so the YSZ peak was stronger than that of LSM even though the source of the signal was buried. After the silver nanoparticles were applied, the LSM peaks significantly grew in size, while the intensity of YSZ remained roughly the same. Therefore, the Ag treatment granted some level of surface specificity to the Raman analysis since only the signal from the thin film on top was visibly enhanced. This feature can provide a capability to detect phase evolution on the cathode surface with superior surface sensitivity, potentially contributing to studies on cathode degradation.

Again, the enhancement in sensitivity to cathode materials (LSCF and LSM) has important implications. To date, the development of new electrode materials for SOFC is still

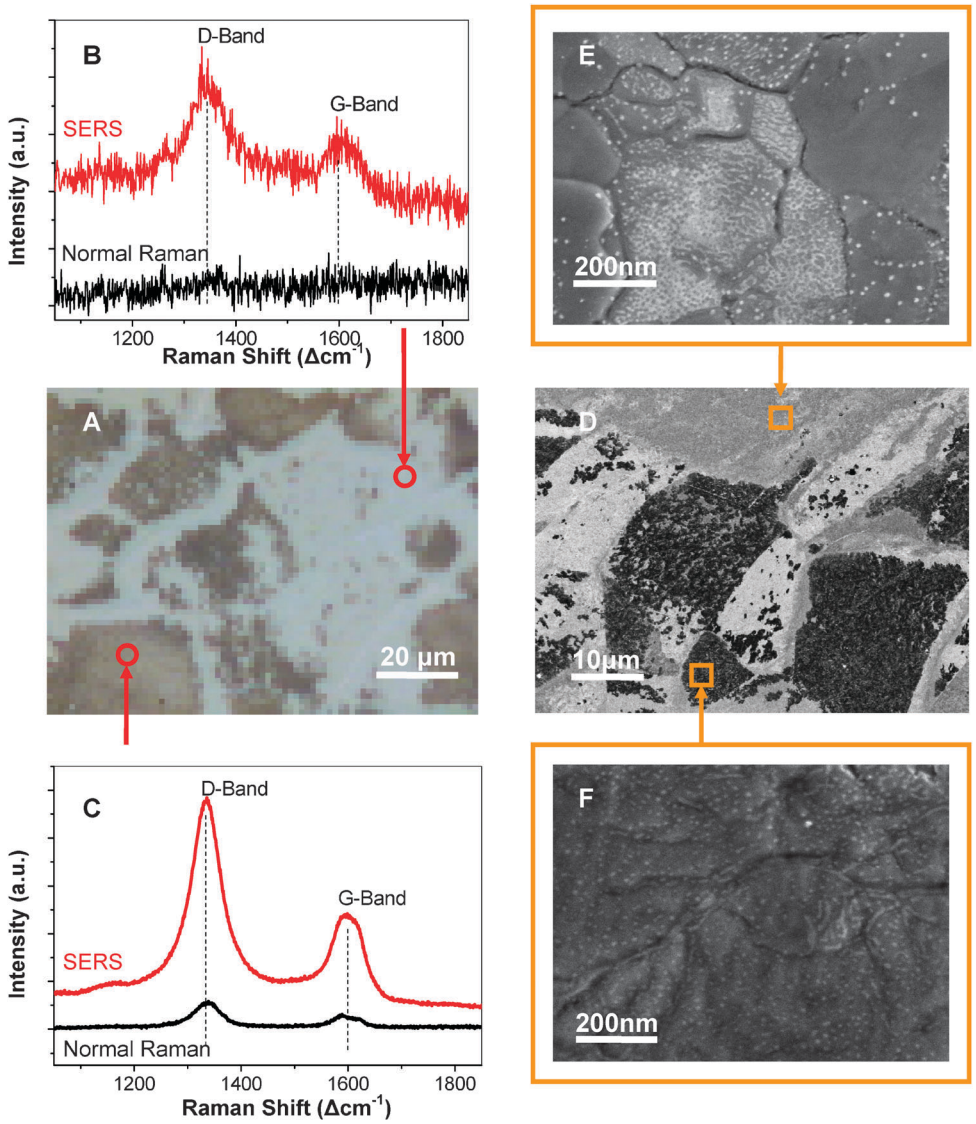

Fig. 3 SERS effect on the hydrocarbon-exposed nickel surface. (A) Hydrocarbon-exposed nickel surface under an optical microscope and (D) the SEM picture with low magnification, both showing the patches of carbon deposition. (B) The Raman spectroscopy of the light region and (C) of the dark region before and after silver sputtering. (E) The high magnification SEM of the light region and (F) of the dark region. SEM images D, E, and F were taken before any silver deposition. All Raman spectra were collected with 633 nm laser, and the silver deposition duration was 180 s.

largely based on experience and intuition rather than scientific models, due largely to the lack of a fundamental understanding of the electrode processes, which are determined by the chemistry and structure of electrode surfaces. It is hoped that SERS with high sensitivity to electrode materials may be a powerful probe to surface composition and structure of electrode, providing critical information for unraveling the mechanism of electrode processes.

In summary, SERS active silver nanoparticles were fabricated through DC sputtering. By using pre-deposited carbon films as the standards, the net enhancement factors were systematically evaluated. Through exploration of the sputter parameters, an optimal condition was found that gives 14 times of net enhancement. Furthermore, the enhancement factor evaluated by R6G molecules was about 4×10^5, comparable to the value attained in previous studies. The optimal SERS treatment was applied to real SOFC materials. By applying SERS sputtered silver onto the nickel surface after hydrocarbon exposure, the carbon signal was enhanced by 8–9 times. Carbon peaks appeared at some regions where it was absent before silver loading. The application in LSM and LSCF showed distinctly enhanced Raman signals after silver sputtering, manifesting the potential to the application on general cathode materials. Our technique demonstrated the capability of detecting surface species present in trace amounts on SOFC electrode surfaces and as well a good surface specificity, which are critical for the future research to understand the catalysis and degradation mechanism of SOFC electrodes.

Direct application of SERS for high temperature fuel cell systems[35] is an attractive direction for further study. However, the coinage metal nanoparticles treated by high temperature usually lose their activity for Raman enhancement, mostly due to the agglomeration and shape change.[36] We noticed the recent development of SERS substrates with inert robust

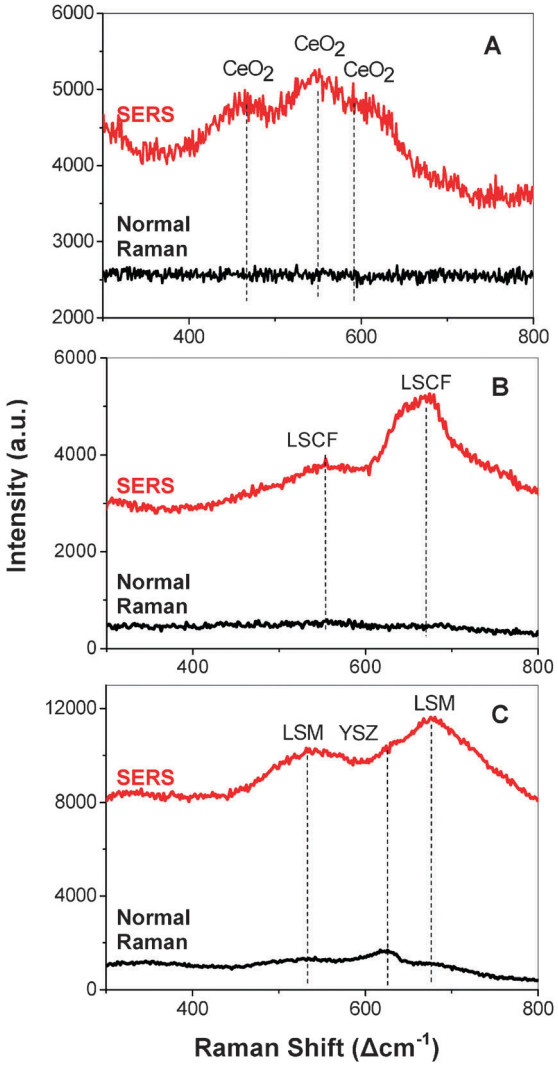

Fig. 4 The normal Raman and SERS spectra collected from (A) CeO_2 loaded on nickel foil, (B) an LSCF pellet, and (C) LSM film sputtered on a YSZ pellet. (A) was collected with red laser excitation (633 nm), while (B) and (C) were excited with green laser (514 nm).

coating (*e.g.* Al_2O_3 or SiO_2)[37–39] that can sustain high temperature or other harsh environments without agglomeration or shape change. These techniques will be further explored in future work for the *in situ* characterization of SOFC electrodes and general electrochemical interfaces.

Acknowledgements

This work was supported by the HeteroFoaM Center, an Energy Frontier Research Center funded by the U.S. DOE, Office of Science, Office of Basic Energy Sciences (BES) under Award Number DE-SC0001061.

References

1 N. Q. Minh and T. Takahashi, *Science and Technology of Ceramic Fuel Cells*, Elsevier, Amsterdam, 1995.
2 L. Yang, Y. Choi, W. Qin, H. Chen, K. Blinn, M. Liu, P. Liu, J. Bai, T. A. Tyson and M. Liu, *Nat. Commun.*, 2011, **2**, 357.
3 L. F. Nie, M. F. Liu, Y. J. Zhang and M. L. Liu, *J. Power Sources*, **195**, 4704–4708.
4 X. Y. Lou, S. Z. Wang, Z. Liu, L. Yang and M. L. Liu, *Solid State Ionics*, 2009, **180**, 1285–1289.
5 M. E. Lynch, L. Yang, W. Qin, J.-J. Choi, M. Liu, K. Blinn and M. Liu, *Energy Environ. Sci.*, **4**, 2249–2258.
6 A. Atkinson, S. Barnett, R. J. Gorte, J. T. S. Irvine, A. J. Mcevoy, M. Mogensen, S. C. Singhal and J. Vohs, *Nat. Mater.*, 2004, **3**, 17–27.
7 Z. Cheng, J.-H. Wang, Y. Choi, L. Yang, M. C. Lin and M. Liu, *Energy Environ. Sci.*, 2011, **4**, 4380–4409.
8 Z. Cheng and M. Liu, *Solid State Ionics*, 2007, **178**, 925–935.
9 Z. Cheng, H. Abernathy and M. L. Liu, *J. Phys. Chem. C*, 2007, **111**, 17997–18000.
10 K. S. Blinn, H. W. Abernathy and M. Liu, in *Advances in Solid Oxide Fuel Cells V*, ed. N. P. S. P. Bansal, vol. 30, pp. 65–73.
11 M. B. Pomfret, J. C. Owrutsky and R. A. Walker, *Anal. Chem.*, 2007, **79**, 2367–2372.
12 M. B. Pomfret, J. C. Owrutsky and R. A. Walker, *J. Phys. Chem. B*, 2006, **110**, 17305–17308.
13 Z. Cheng, S. Zha and M. Liu, *J. Electrochem. Soc.*, 2006, **153**, A1302–A1309.
14 X. Y. Lu, P. W. Faguy and M. L. Liu, *J. Electrochem. Soc.*, 2002, **149**, A1293–A1298.
15 X. Lu, P. Faguy, C. Xia and M. Liu, *Proc. – Electrochem. Soc.*, 2000, **32**, 401–407.
16 Y. M. Choi, H. Abernathy, H. T. Chen, M. C. Lin and M. L. Liu, *ChemPhysChem*, 2006, **7**, 1957–1963.
17 L. Yang, S. Wang, K. Blinn, M. Liu, Z. Liu, Z. Cheng and M. Liu, *Science*, 2009, **326**, 126–129.
18 P. L. Stiles, J. A. Dieringer, N. C. Shah and R. R. Van Duyne, *Annu. Rev. Anal. Chem.*, 2008, **1**, 601–626.
19 J. A. Dieringer, K. L. Wustholz, D. J. Masiello, J. P. Camden, S. L. Kleinman, G. C. Schatz and R. P. Van Duyne, *J. Am. Chem. Soc.*, 2009, **131**, 849–854.
20 Z. Q. Tian, J. S. Gao, X. Q. Li, B. Ren, Q. J. Huang, W. B. Cai, F. M. Liu and B. W. Mao, *J. Raman Spectrosc.*, 1998, **29**, 703–711.
21 Z. Q. Tian, B. Ren, J. F. Li and Z. L. Yang, *Chem. Commun.*, 2007, 3514–3534.
22 J. Lee, S. Shim, B. Kim and H. S. Shin, *Chem.–Eur. J.*, **17**, 2381–2387.
23 F. Schedin, E. Lidorikis, A. Lombardo, V. G. Kravets, A. K. Geim, A. N. Grigorenko, K. S. Novoselov and A. C. Ferrari, *ACS Nano*, **4**, 5617–5626.
24 K. L. A. Chan and S. G. Kazarian, *Nanotechnology*, **22**, 5.
25 R. G. Freeman, K. C. Grabar, K. J. Allison, R. M. Bright, J. A. Davis, A. P. Guthrie, M. B. Hommer, M. A. Jackson, P. C. Smith, D. G. Walter and M. J. Natan, *Science*, 1995, **267**, 1629–1632.
26 Y. Liu, S. Zha and M. Liu, *Adv. Mater. (Weinheim, Ger.)*, 2004, **16**, 256–260.
27 R. Gupta, M. J. Dyer and W. A. Weimer, *J. Appl. Phys.*, 2002, **92**, 5264–5271.
28 S. Schelz, T. Richmond, P. Kania, P. Oelhafen and H. J. Guntherodt, *Surf. Sci.*, 1996, **359**, 227–236.
29 N. E. Marotta, J. R. Barber, P. R. Dluhy and L. A. Bottomley, *Appl. Spectrosc.*, 2009, **63**, 1101–1106.
30 R. M. Stockle, V. Deckert, C. Fokas and R. Zenobi, *Appl. Spectrosc.*, 2000, **54**, 1577–1583.
31 H. Takahashi, T. Takeguchi, N. Yamamoto, M. Matsuda, E. Kobayashi and W. Ueda, *J. Mol. Catal. A: Chem.*, **350**, 69–74.
32 H. Kurokawa, T. Z. Sholklapper, C. P. Jacobson, L. C. De Jonghe and S. J. Visco, *Electrochem. Solid-State Lett.*, 2007, **10**, B135–B138.
33 L. W. Tai, M. M. Nasrallah, H. U. Anderson, D. M. Sparlin and S. R. Sehlin, *Solid State Ionics*, 1995, **76**, 273–283.
34 J. F. Mitchell, D. N. Argyriou, C. D. Potter, D. G. Hinks, J. D. Jorgensen and S. D. Bader, *Phys. Rev. B: Condens. Matter Mater. Phys.*, 1996, **54**, 6172–6183.
35 T. Itoh, T. Maeda and A. Kasuya, *Faraday Discuss.*, 2006, **132**, 95–109.
36 K. R. Beavers, N. E. Marotta and L. A. Bottomley, *Chem. Mater.*, **22**, 2184–2189.
37 A. V. Whitney, J. W. Elam, P. C. Stair and R. P. Van Duyne, *J. Phys. Chem. C*, 2007, **111**, 16827–16832.
38 E. V. Formo, S. M. Mahurin and S. Dai, *ACS Appl. Mater. Interfaces*, **2**, 1987–1991.
39 J. F. Li, Y. F. Huang, Y. Ding, Z. L. Yang, S. B. Li, X. S. Zhou, F. R. Fan, W. Zhang, Z. Y. Zhou, D. Y. Wu, B. Ren, Z. L. Wang and Z. Q. Tian, *Nature*, **464**, 392–395.